FRONTIERS OF PHYSICS

LETTER
Volume 19 / Issue 6 / 63210 / 2024

Strong ferroelectricity in one-dimensional materials self-assembled by superatomic metal halide clusters

Yu Guo[1], Yang Zhao[1], Qiao Ling[1], Si Zhou[1,2,3,†], Jijun Zhao[1,2,3,‡]

1 Key Laboratory of Materials Modification by Laser, Ion and Electron Beams (Dalian University of Technology), Ministry of Education, Dalian 116024, China
2 Guangdong Provincial Key Laboratory of Quantum Engineering and Quantum Materials, School of Physics, South China Normal University, Guangzhou 510006, China
3 Guangdong-Hong Kong Joint Laboratory of Quantum Matter, Frontier Research Institute for Physics, South China Normal University, Guangzhou 510006, China
Corresponding authors. E-mail: †sizhou@dlut.edu.cn, ‡zhaojj@dlut.edu.cn
Received December 19, 2023; accepted June 16, 2024

ABSTRACT

Cluster-assembled materials have long been pursued as they can create some unprecedented and desirable properties. Herein, we assemble a class of one-dimensional (1D) $ReNX_4$ (X = F, Cl, Br and I) and MF_5 (M = V, Nb and Ta) nanowires by covalently linking their superatomic clusters. These assembled 1D nanowires exhibit outstanding energetic and dynamic stabilities, and hold sizable spontaneous polarization, low ferroelectric switching barriers and high critical temperature. Their superior ferroelectricity is originated from d^0-configuration transition metal ions generated by the hybridization of empty d orbitals of metal atoms and p orbitals of non-metal atoms. These critical insights pave a new avenue to fabricate 1D ferroelectrics toward the development of miniaturized and high-density electronic devices using building blocks as cluster with precise structures and functionalities.

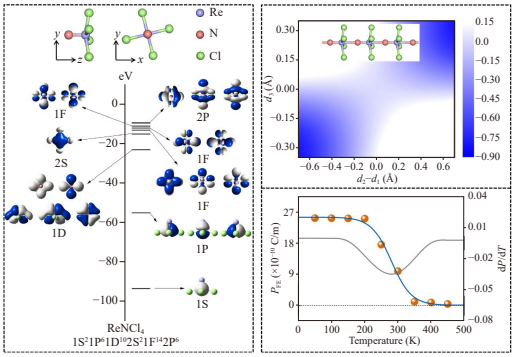

Keywords ferroelectricity, superatom, cluster-assembled materials, electronic properties, first-principles calculations

1 Introduction

Ferroelectric (FE) materials with the emergence of spontaneous electric polarization, have a wide range of technological applications, such as non-volatile memories, field effect transistors, sensors, and photovoltaics [1–5]. However, miniaturizing FE devices suffers from size limitation of the FE materials due to internal depolarizing electrostatic fields [6]. To overcome this issue, significant progress has been made in two-dimensional (2D) ferroelectrics. The ferroelectric polarization in 2D materials of atomic thickness can be strong enough to subsist, offering a natural solution for nanoscale ferroelectric applications [7, 8].

The lateral dimensionality of 2D ferroelectrics is formally infinite. In reality, however, the ferroelectricity may be weakened by edge reconstruction and boundary [9]. Alternatively, one-dimensional (1D) materials with "no-boundary" feature might be more appropriate for ferroelectrics. So far, several 1D FE nanostructures have been prepared in the laboratory, such as tetrabromo-p-benzoquinone chain [10, 11], water molecules in quasi-1D beryl crystal [12], $BaTiO_3$ and $PbTiO_3$ nanotubes [13], which, however, intrinsically contain nonnegligible structural defects. Therefore, it is still desirable to explore 1D ferroelectrics with structurally perfect "boundary" and

https://doi.org/10.1007/s11467-024-1434-3

high stability.

Atomically precise nanoclusters offer new opportunities for exploring excellent properties and can serve as building blocks with tunable electronic structures for assembling materials and devices [14]. Among them, "superatomic clusters" (namely, "superatoms") possess outstanding stability and are promising for self-assembling [15, 16]. Indeed, some superatomic cluster assembled nanomaterials have already been synthesized. For instance, Re_6Se_8 clusters can be assembled into a 2D hierarchical semiconductor via strong interaction by substitutionally labile Cl atoms, whose transport properties are tunable from semiconducting to metallic and to superconducting upon *n*-type doping through Cl dissociation [17–19]. C_{60} together with $Co_6Se_8/Cr_6Te_8/Ni_6Te_8$ clusters were patterned into three-dimensional crystalline array with CdI_2 or NaCl type [20]. On the theoretical side, Guo *et al.* [21] proposed a strategy to construct stable 2D lattices using superatomic tetrahedral clusters (i.e., B_4, Al_4, Ga_4, In_4, Cr_4, Mo_4, and Te_4) covalently linked by oxygen atoms. Du *et al.* [22] examined 27 dimers of endohedral cage clusters and predicted that $M@X_{16}$ (M = Ti, Zr, or Hf; X = Si, Ge, or Sn) are potential zero-dimensional vdW Lego blocks. Xing *et al.* [23, 24] presented a joint experiment-theory investigation of a rationally designed layered superatomic crystal of $Au_6Te_{12}Se_8$ cubes stacked by noncovalent intercube quasibonds, finding a sequential-emerged anisotropic triple-cube charge density wave and polarized metallic states below 120 K. Zhao *et al.* [25] designed a series of fullerene-based 1D chains, namely $U_2C@C_{80}$-M (M = Cr, Mn, Mo, and Ru) 1D chains, with both ferroelectric and ferromagnetic properties.

$ReNCl_4$ cluster with nearly ideal C_{4v} symmetry has been synthesized in a facile synthesis from perrhenate, sodium azide and HCl gas [26–28]. Inspired by the aforementioned cluster assemblies with extraordinary properties, herein we design 1D nanowires of $ReNX_4$ (X = F, Cl, Br, and I) by cluster self-assembling and extend them to 1D nanowires of MF_5 (M = V, Nb, and Ta) by isoelectronic substitution. The cluster-assembling rule takes into account both the closed electronic shells for $ReNX_4$ and MF_5 clusters as well as the binding strength between metal and N/F atoms. The molecular orbitals and superatomic characters of these clusters with 40 valence electrons were identified for the first time. Owing to second-order Jahn–Teller effect, these assembled nanowires intrinsically hold superior ferroelectricity with Curie temperature above 300 K, thereby paving a new route for the design of intrinsic 1D ferroelectrics from self-assembling.

2 Computational methods

Density functional theory (DFT) calculations were performed using the Vienna *ab initio* simulation package (VASP) [29], with planewave basis set (energy cutoff of 500 eV), projector augmented wave potentials [30], and Perdew–Burke–Ernzerhof (PBE) exchange–correlation functional [31]. Based on equilibrium structures, a hybrid HSE06 functional [32] was further used to compute the electronic band structures. The convergence criteria for total energy and force were set to 10^{-7} eV and 0.01 eV·Å^{-1}, respectively. Uniform **k**-point meshes with spacing of ~0.015 Å^{-1} were adopted to sample the Brillouin zones. Phonon dispersion analysis was performed using the Phonopy code [33] based on the density functional perturbation theory. The frontier molecular orbitals and natural population of individual $ReNX_4$ and MF_5 clusters were analyzed using the PBE functional accompanied with 6-311+G(d) [34] and SDD [35] basis sets, implemented in Gaussian16 suite [36].

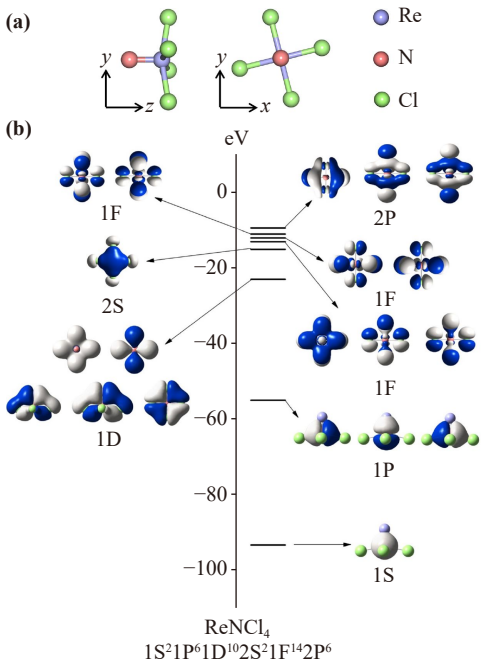

Fig. 1 **(a)** Atomic structure of $ReNCl_4$ cluster. **(b)** Molecular orbitals referred to the vacuum energy level as zero and a classification of orbital pattern into superatomic 1S, 1P, 1D, 2S, 1F and 2P states for $ReNCl_4$ cluster. Blue and red colors denote positive and negative phases of the wavefunction, respectively. The isosurface value is ±0.05 a.u. The Re, N and Cl atoms are shown in purple, pink and green colors, respectively.

3 Results and discussion

We firstly investigate the atomic structure and electronic properties of an individual $ReNCl_4$ cluster. As shown in Fig. 1(a), four equivalent Cl^- atoms and one N^{3-} atom are bonded with one Re^{7+} atom to form a stable N–Re–Cl_4 unit with C_{4v} symmetry, with N–Re and

Table 1 Lattice parameters a, off-center displacement (d_2–d_1 and d_3) of metal along the axial z direction, formation energy E_f, band gaps E_g, potential barrier of E_B, spontaneous polarization P_{FE}, Curie temperature T_C, piezoelectric response e_{11} and pyroelectric response p.

Materials	$ReNF_4$	$ReNCl_4$	$ReNBr_4$	$ReNI_4$	VF_5	NbF_5	TaF_5
a (Å)	4.10	4.08	4.04	3.88	4.63	4.23	4.11
d_2–d_1 (Å)	0.74	0.70	0.63	0.41	0.82	0.40	0.20
d_3 (Å)	0.32	0.36	0.35	0.28	0.43	0.34	0.21
E_f (eV)	–0.28	–0.22	–0.28	–0.43	–0.10	–0.12	–0.18
E_g (eV)	4.25 (d)	2.25	1.43	--	4.94 (d)	6.97	6.60
E_B (eV)	0.74	0.81	0.85	--	0.50	0.10	0.09
P_{FE} (10^{-10} C/m)	52.03	25.64	28.58	--	55.5	24.64	36.96
T_C (K)	224	280	321	--	95	86	72
e_{11} (10^{-10} C/m)	30.29	22.86	22.21	--	35.47	31.47	61.28
p (10^{-10} C/(K·m^{-2}))	0.06	0.02	0.02	--	0.13	0.07	0.12

Re–Cl bond length of 1.67 and 2.30 Å, respectively, and Cl–Re–N angle of 81.24°. According to the valence electronic configurations of Re ($5d^5 6s^2$), N ($2s^2 2p^3$) and Cl ($3s^2 2p^5$) atoms, each $ReNCl_4$ cluster carry totally 40 valence electrons and achieves a closed electronic shell of $1S^2 1P^6 1D^{10} 2S^2 1F^{14} 2P^6$, which is evidently demonstrated in Fig. 1(b). For the first time, the superatomic characteristics [37] for valence molecular orbitals of $ReNCl_4$ cluster are identified, suggesting its great potential as a building block to assemble nanomaterial.

According to the geometric feature of $ReNCl_4$ cluster, Re atom is prone to bond with another N atom in adjacent $ReNCl_4$ cluster to form distorted corner-sharing ReN_2Cl_4 octahedra without tilt. In this manner, $ReNCl_4$ units can be self-assembled to construct a $ReNCl_4$ wire along the z axial direction with $P4$ symmetry and 1D lattice parameter of 4.08 Å. Here, each N^{3-} ion is bonded in a distorted linear geometry to two Re^{7+} atoms and each Cl^- ion is bonded to one Re^{7+} atom with bond length of 2.31 Å, resulting in invariable valence states of Re, N and Cl atoms as confirmed via the analysis of on-site Bader charge [38] (Re: –2.1e; N: 0.9e; Cl: 0.3e). There are one shorter (1.69 Å) and one longer (2.30 Å) Re–N bond with bond overlap population [39] of 0.93 and 0.11, corresponding to nature of strong and weak covalent bond respectively.

To verify the energetic stability of $ReNCl_4$ nanowire, we calculate its formation energy ΔH defined as $\Delta H = E_{wire} - E_{cluster}$, where E_{wire} and $E_{cluster}$ are the energy for one unit of 1D nanowire and an individual cluster, respectively. $ReNCl_4$ nanowire shows negative ΔH of –0.22 eV per formula (Table 1), indicating that its formation is exothermic. The kinetic stability of $ReNCl_4$ nanowire is also confirmed by the phonon dispersions in Fig. 2(b).

In light of the stability of self-assembled $ReNCl_4$ nanowire, Cl atoms can be substituted by other halogens (X = F, Br and I) and a series of hypothetic 1D $ReNX_4$ compounds might possess analogous structure as $ReNCl_4$

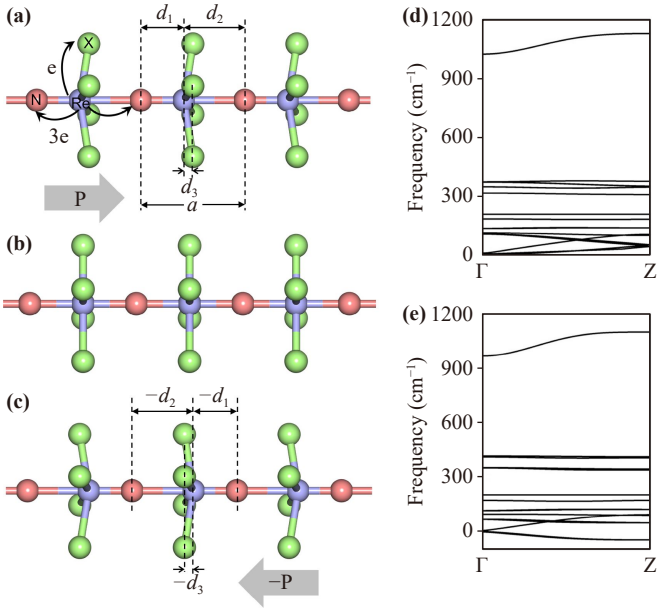

Fig. 2 Atomic structures of cluster-assembled nanowires with **(a)** FE, **(b)** PE and **(c)** –FE state, respectively. The Re (or V, Nb and Ta), N (or F) and Cl (or F and Br) atoms are shown in purple, pink and green colors, respectively. d_1 and d_2 represents the bond length of metal-linked atoms, and d_3 represents displacements of metal and halogen atoms along (001) chain direction. Phonon spectrum of **(d)** FE and **(e)** PE phase of $ReNCl_4$ nanowire, respectively.

nanowire. More importantly, all these $ReNX_4$ clusters exhibit superatomic characters. Additionally, isoelectronic substitution is another effective strategy to design isostructural materials. Note that MX_5 (M = V, Nb and Ta; X = Cl, F, Br and I) hold same number of valence electrons with that of $ReNCl_4$ (40e), resulting in similar geometric structure for both types of clusters, that is, MX_5 cluster also displays X–M–X_4 arrangement like $ReNCl_4$ cluster. Therefore, 1D distorted MX_5 nanowires can be also constructed by self-assembling of MX_5 clusters (see Fig. 2). The energetic and dynamical stabilities of

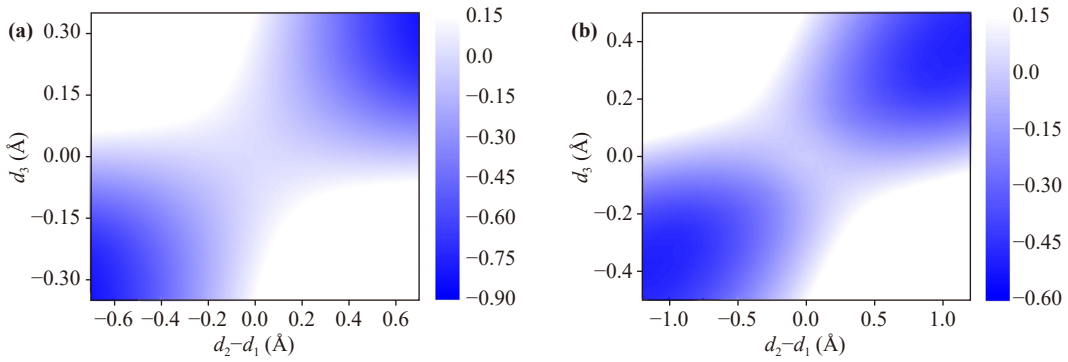

Fig. 3 The energy contour plot (in eV) of 1D **(a)** $ReNCl_4$ and **(b)** VF_5 unit cell as a function of polar displacements of the metal ions. The energy of the PE phase is set to zero.

these predicted nanowires are systematically assessed by their formation energies and phonon dispersions [Fig. S1 of the Electronic Supplementary Materials (ESM)]. Eventually, we screen out $ReNF_4$, $ReNCl_4$, $ReNBr_4$, $ReNI_4$, VF_5, NbF_5 and TaF_5 nanowires with exothermic formation energies ranging from –0.01 to –0.43 eV per formula, suggesting experimental feasibility for the synthesis of these 1D structures via cluster self-assembling. These results also support that self-assembling superatomic clusters is beneficial for thermodynamic stability. Specifically, the lattice parameters of $ReNX_4$ nanowires in the range of 3.88–4.10 Å are smaller than 4.11–4.63 Å for MF_5 nanowires (Table 1). In addition, the lattice constant of $ReNX_4$ (MF_5) nanowire decreases with increasing atomic number of X (M) element. In all situations, metal ions show an off-center displacement along z axial direction by 0.20–0.82 Å. The electronic band structures of $ReNX_4$ and MF_5 nanowires are depicted in Fig. S2 of the ESM. Expect $ReNI_4$, all assembled nanowires are semiconductors with moderate or wide band gaps, which allows switching of the polarization a ferroelectric by applying an external field.

Due to non-centrosymmetry of $ReNX_4$ and MF_5 nanowires, there is spontaneous polarization along z axial direction. In order to explore the ferroelectric feature of these 1D nanowires, the centrosymmetric phase ($P4/m$ symmetry) without displacement between metal and halide atoms along z axis is firstly identified as the paraelectric (PE) configuration (Fig. 2). As a representative, Fig. 2(c) displays the phonon dispersion of 1D PE $ReNCl_4$. Here, three imaginary branches including acoustic and optical phonon modes are throughout the entire Brillouin zone, indicating the geometric instability of PE configuration and a tendency of phase transition from ferroelectric state to a paraelectric state below Curie temperature (T_C). In addition, PE phase has higher energy than that of FE phase by 0.09–0.85 eV per formula. Taking $ReNCl_4$ and VF_5 nanowires as examples, the scanned free-energy contour is plotted with different values of d_2–d_1 and d_3 in Fig. 3 (d_1 and d_2 represent the bond length of metal-linked atoms, and d_3 represents displacements of metal and halogen atoms along z chain direction). FE and –FE phases are equivalent states with lowest energy, separated by the nonpolar PE state ($d_2 - d_1 = d_3 = 0$) located at the diagonal direction. These indicate the higher stability of FE and –FE phases compared with PE phase. The energy maps of other nanowires are presented in Fig. S3 of the ESM, showing similar phenomena.

The central symmetry of 1D FE $ReNX_4$ and MF_5 nanowires is eliminated due to the cooperative displacements between metal and halogen atoms, resulting in an evident spontaneous polarization P_{FE} along the chain direction. According to Berry phase through the modern theory of polarization [40], the calculated P_{FE} of 1D FE $ReNX_4$ and MF_5 nanowires are $(25.64–52.03)\times 10^{-10}$ C/m and $(24.64–55.50)\times 10^{-10}$ C/m, respectively, which are comparable and even larger than the values of many FE materials, such as transition-metal dichalcogenides [41], group-IV monochalcogenides [42, 43], bulk $BaTiO_3$ [44, 45] and lead-zirconate-titanate (PZT) [46, 47].

We further explore the origin of ferroelectricity in these nanowires. 1D $ReNX_4$ and MF_5 are semiconductors with band gaps in range of 1.43–1.25 eV and 4.94–6.60 eV, respectively, and display similar features of electronic structure (Fig. S2 of the ESM). Note that $ReNF_4$ and VF_5 possess direct band gaps. Taking 1D FE $ReNCl_4$ nanowire as representative, the projected density of states for each element are displayed in Fig. 4. The hybridization between Re–d_{xz}/d_{yz}, N–p_z and Cl–p_z near the Fermi level is originated from Re–Cl and Re–N bonding. Here, the cooperation of empty d orbitals for Re^{5+} and p orbitals for N^{3-} along the polar direction regulates the existence of FE states in 1D $ReNCl_4$, resulting in the second-order Jahn–Teller effect aroused by d^0-configuration [48, 49], which is similar with the well-known FE perovskite oxides [44, 50]. Analogously, the ferroelectricity of VF_5 nanowire also results from d^0 principle generated by V^{5+} empty d orbitals. Furthermore, more remarkable $pd\pi$ interaction of Re–$d_{xz/yz}$/N–$p_{x/y}$ than $pd\sigma$ interaction signifies the strong ferroelectric

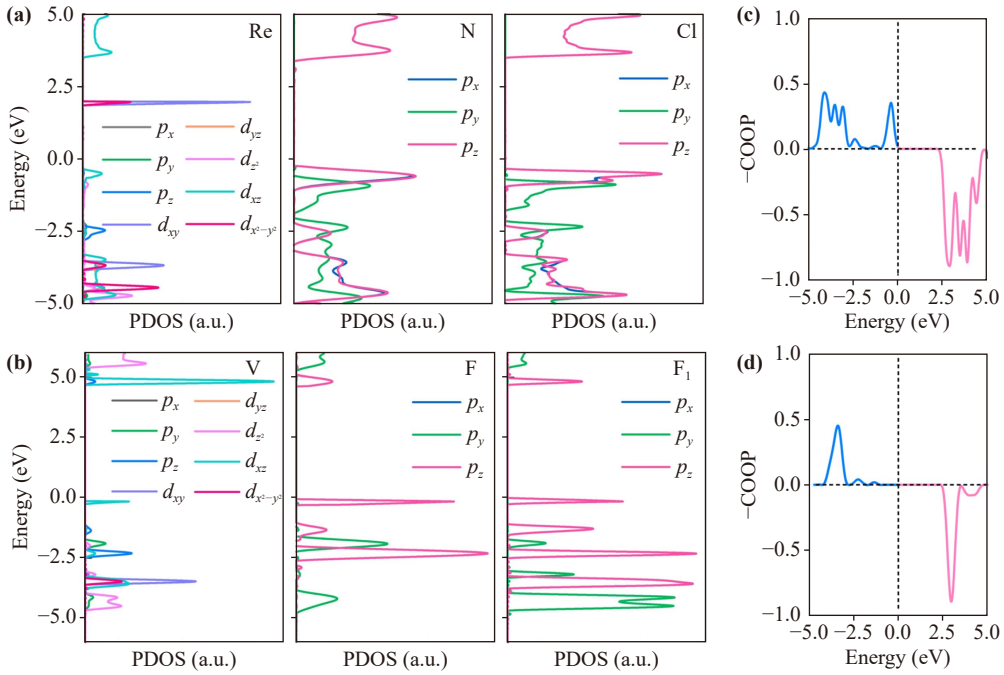

Fig. 4 The PDOS of **(a)** $ReNCl_4$ and **(b)** VF_5. Here, F is the atom linking two clusters and four F_1 atoms are located at xy plane. –COOP curves for **(c)** $ReNCl_4$ and **(d)** VF_5.

effect, which is also appeared in $BaTiO_3$ and $PbTiO_3$ [44]. Figures 4(c, d) and Fig. S4 of the ESM present the –COOP (Crystal Orbital Overlap Population) integrals for Re–N and M–F bonds, where a positive –COOP denotes favorable bonding interaction and a negative –COOP indicates unfavorable antibonding interaction. The results reveal that the occupied states are bonding states, while the unoccupied states belong to antibonding ones, further confirming that the FE states is stabilized by Re–N and M–F bonding.

Within the Landau–Ginzburg theory [51], the free energy and polarization should satisfy $E = \sum_i \left[\frac{\alpha}{2}(P_i)^2 + \frac{\beta}{2}(P_i)^4\right] + \frac{\gamma}{2}\sum_{i,j}(P_i - P_j)^2$. The first two terms are related to the energy contribution to polarization in each unit cell, which can be described by anharmonic double-well shape of the potential profile. α and β parameters are obtained by fitting the double-well potentials in Fig. 5 and Fig. S5 of the ESM. The third term reflects the nearest-neighbor dipole–dipole coupling within the nanowire, and coefficient γ is fitted using the mean-field theory within nearest-neighbor approximation, which can be plotted as a parabola shape in second-order approximation shown in Fig. 5(b) and Fig. S6 of the ESM. The energy barrier E_B for the transition from ferroelectric to paraelectric phases of $ReNX_4$ and MF_5 nanowires can be determined as 0.74–0.85 eV and 0.09–0.50 eV, respectively. It is noteworthy that E_B is one order of magnitude larger than that of other frequently used ferroelectrics such as $BaTiO_3$ and $PbTiO_3$ [44], suggesting high Curie temperature for these ferroelectric nanowires.

Ab initio molecular dynamic (AIMD) simulations [52] with 1×1×8 supercells are also performed to evaluate the Curie temperature of these nanowires. Figure 5(c) and Fig. S7 of the ESM show P_{FE} as a function of temperature. Taking $ReNCl_4$ and VF_5 nanowires as representatives, the static P_{FE} values of 25.64 C/m and 55.50 C/m are maintained at finite temperature up to about 300 and 100 K, respectively. Then the Curie temperature for transition of FE to PE phases can be fitted as the temperature-dependent $P(T) = a/(1+e^{-k(T-T_C)})$, where a and k are constants. Importantly, T_C value is usually related to the energy barrier E_B and the dipole–dipole coupling between the adjacent unit cells, that is, T_C increases with increasing E_B. Here, $ReNX_4$ nanowires with larger E_B results in higher T_C value (224–321 K) compared with MF_5 nanowires (72–95 K), which also can be obtained from the pyroelectric response defined as $p = -(dP/dT)$. Moreover, the piezoelectric response e_{11} is dependent on a linear fitting of 1D polarization changes with respect to the uniaxial strains ε_{11} along the z direction. A linear relation between polarization change and the strain within ±1% for $ReNX_4$ and MF_5 nanowires has been demonstrated in Fig. 5(d) and Fig. S8 of the ESM. The obtained e_{11} is as high as 61×10^{-10} C/m, which is an order of magnitude larger than that of MoS_2 monolayer (3.64×10^{-10} C/m) [53]. The active pyroelectric and piezoelectric responses in these nanowires suggest their broad applications in sensors and energy conversion devices. Particularly, the giant pyroelectric coefficients of $ReNX_4$ and MF_5

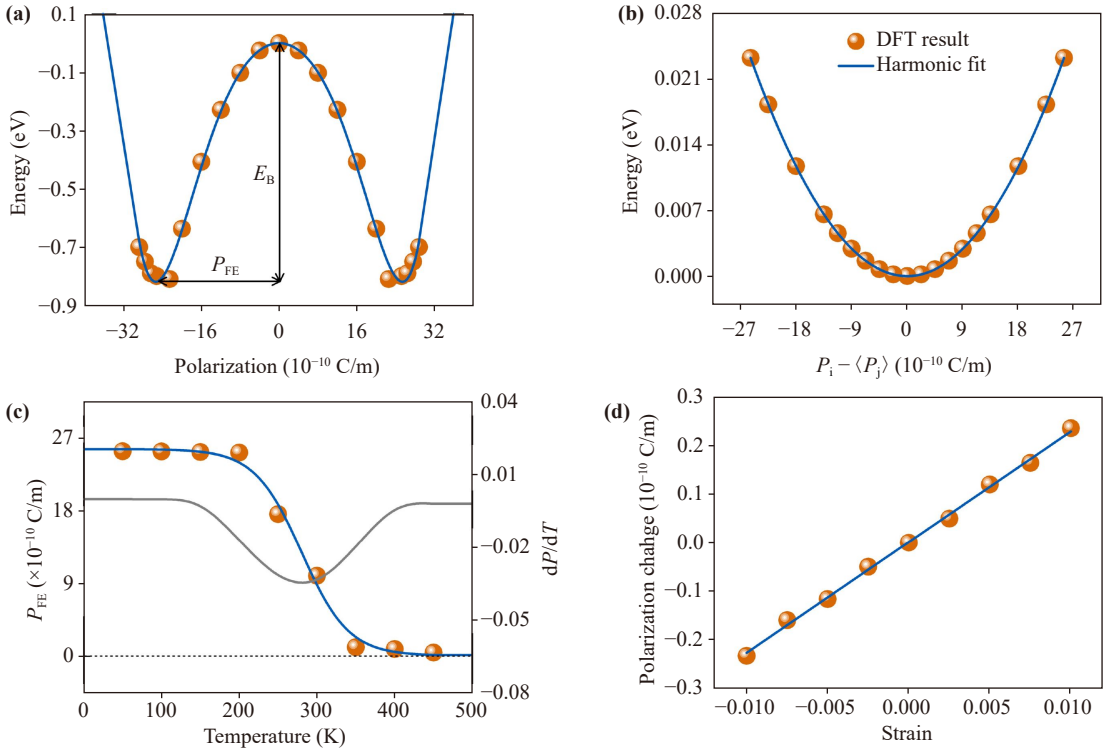

Fig. 5 **(a)** Double-well potential versus polarization for $ReNCl_4$ nanowire. E_B is the potential barrier. **(b)** The dipole-dipole interaction energy for $ReNCl_4$ nanowires calculated by the mean-field method. **(c)** Temperature dependence of polarization obtained from *ab initio* molecular dynamics (orange balls). Blue line is a sigmoid fit to MD results and grey line is the pyroelectric response (dP/dT) for $ReNCl_4$ nanowire. **(d)** Piezoelectric response (relaxed-ion e_{11} coefficient) for $ReNCl_4$ nanowire from DFT calculations. The polarization and strain are all along the x direction. The corresponding relaxed-ion piezoelectric coefficient e_{11} can be obtained from slope of the line.

nanowires in range of $(0.02–0.13)\times10^{-10}$ C/(K·m^2) (Table 1) are larger than those of most ferroelectric crystals, for instance, 2.0, 8.3, and 1.8×10^{-4} C/(K·m^2) for $BaTiO_3$, $LiNbO_3$ and $LiTaO_3$, respectively [54].

4 Conclusion

In summary, we have designed a series of $ReNX_4$ (X = F, Cl, Br and I) and MF_5 (M = V, Nb and Ta) nanowires by self-assembling superatomic clusters, based on the criteria of superatomic orbital characters within the shell model and orbital interaction between adjacent clusters. Self-assembling superatomic clusters can strengthen the stability of these 1D structures and achieve ferroelectric effect. These cluster-self-assembled 1D materials are all dynamically stable and possess a moderate or wide band gap of 1.43–6.60 eV (expect for metallic $ReNI_4$ nanowire). Notably, $ReNX_4$ and MF_5 nanowires exhibit sizable spontaneous polarization and low switching barrier, and $ReNX_4$ nanowires hold high T_C above room temperature that is essential for ferroelectric devices. The extraordinary ferroelectric properties in these assembled materials are derived from an electronic mechanism, i.e., the second-order Jahn–Teller effect with d^0-configuration transition-metal ions in the materials. These theoretical results open unprecedented opportunities for the discovery of new ferroelectric materials and point to a feasible route for the exploration of exotic 1D physics from cluster assemblies.

Declarations The authors declare that they have no competing interests and there are no conflicts.

Electronic supplementary materials The online version contains supplementary material available at https://doi.org/10.1007/s11467-024-1434-3 and https://journal.hep.com.cn/fop/EN/10.1007/s11467-024-1434-3.

Acknowledgements This work was supported by the National Natural Science Foundation of China (Nos. 12004065, 91961204, 12222403, and 11974068), the Doctoral Start-up Foundation of Liaoning Province (No. 2022-BS-081), and the Fundamental Research Funds for the Central Univeristies (No. DUT24LAB114).

References

1. K. Zhang, C. Wang, M. Zhang, Z. Bai, F. F. Xie, Y. Z. Tan, Y. Guo, K. J. Hu, L. Cao, S. Zhang, X. Tu, D.

Pan, L. Kang, J. Chen, P. Wu, X. Wang, J. Wang, J. Liu, Y. Song, G. Wang, F. Song, W. Ji, S. Y. Xie, S. F. Shi, M. A. Reed, and B. Wang, A Gd@C82 single-molecule electret, *Nat. Nanotechnol.* 15(12), 1019 (2020)
2. J. Müller, T. Böscke, D. Bräuhaus, U. Schröder, U. Böttger, J. Sundqvist, P. Kücher, T. Mikolajick, and L. Frey, Ferroelectric $Zr_{0.5}Hf_{0.5}O_2$ thin films for nonvolatile memory applications, *Appl. Phys. Lett.* 99(11), 112901 (2011)
3. M. Si, A. K. Saha, S. Gao, G. Qiu, J. Qin, Y. Duan, J. Jian, C. Niu, H. Wang, W. Wu, S. K. Gupta, and P. D. Ye, A ferroelectric semiconductor field-effect transistor, *Nat. Electron.* 2(12), 580 (2019)
4. P. Muralt, Ferroelectric thin films for micro-sensors and actuators: A review, *J. Micromech. Microeng.* 10(2), 136 (2000)
5. J. Li, S. Hou, Y. R. Yao, C. Zhang, Q. Wu, H. C. Wang, H. Zhang, X. Liu, C. Tang, M. Wei, W. Xu, Y. Wang, J. Zheng, Z. Pan, L. Kang, J. Liu, J. Shi, Y. Yang, C. J. Lambert, S. Y. Xie, and W. Hong, Room-temperature logic-in-memory operations in single-metallofullerene devices, *Nat. Mater.* 21(8), 917 (2022)
6. L. W. Martin and A. M. Rappe, Thin-film ferroelectric materials and their applications, *Nat. Rev. Mater.* 2(2), 16087 (2016)
7. M. Wu and P. Jena, The rise of two-dimensional van der Waals ferroelectrics, *Wiley Interdiscip. Rev. Comput. Mol. Sci.* 8(5), e1365 (2018)
8. C. C. Chiang, V. Ostwal, P. Wu, C. S. Pang, F. Zhang, Z. Chen, and J. Appenzeller, Memory applications from 2D materials, *Appl. Phys. Rev.* 8(2), 021306 (2021)
9. L. Qi, S. Ruan, and Y. J. Zeng, Review on recent developments in 2D ferroelectrics: Theories and applications, *Adv. Mater.* 33(13), 2005098 (2021)
10. S. Horiuchi and Y. Tokura, Organic ferroelectrics, *Nat. Mater.* 7(5), 357 (2008)
11. Y. Tokura, S. Koshihara, N. Iwasawa, and G. Saito, Domain-wall dynamics in organic charge-transfer compounds with one-dimensional ferroelectricity, *Phys. Rev. Lett.* 63(21), 2405 (1989)
12. B. Gorshunov, V. Torgashev, E. Zhukova, V. Thomas, M. Belyanchikov, C. Kadlec, F. Kadlec, M. Savinov, T. Ostapchuk, J. Petzelt, J. Prokleška, P. V. Tomas, E. V. Pestrjakov, D. A. Fursenko, G. S. Shakurov, A. S. Prokhorov, V. S. Gorelik, L. S. Kadyrov, V. V. Uskov, R. K. Kremer, and M. Dressel, Incipient ferroelectricity of water molecules confined to nano-channels of beryl, *Nat. Commun.* 7(1), 12842 (2016)
13. B. A. Hernandez, K. S. Chang, E. R. Fisher, and P. K. Dorhout, Sol–gel template synthesis and characterization of $BaTiO_3$ and $PbTiO_3$ nanotubes, *Chem. Mater.* 14(2), 480 (2002)
14. P. Jena and Q. Sun, Super atomic clusters: Design rules and potential for building blocks of materials, *Chem. Rev.* 118(11), 5755 (2018)
15. J. Zhao, Q. Du, S. Zhou, and V. Kumar, Endohedrally doped cage clusters, *Chem. Rev.* 120(17), 9021 (2020)
16. Z. Luo and A. W. Castleman, Special and general superatoms, *Acc. Chem. Res.* 47(10), 2931 (2014)
17. B. Choi, K. Lee, A. Voevodin, J. Wang, M. L. Steigerwald, P. Batail, X. Zhu, and X. Roy, Two-dimensional hierarchical semiconductor with addressable surfaces, *J. Am. Chem. Soc.* 140(30), 9369 (2018)
18. E. J. Telford, J. C. Russell, J. R. Swann, B. Fowler, X. Wang, K. Lee, A. Zangiabadi, K. Watanabe, T. Taniguchi, C. Nuckolls, P. Batail, X. Zhu, J. A. Malen, C. R. Dean, and X. Roy, Doping-induced superconductivity in the van der Waals superatomic crystal $Re_6Se_8Cl_2$, *Nano Lett.* 20(3), 1718 (2020)
19. X. Zhong, K. Lee, B. Choi, D. Meggiolaro, F. Liu, C. Nuckolls, A. Pasupathy, F. De Angelis, P. Batail, X. Roy, and X. Zhu, Superatomic two-dimensional semiconductor, *Nano Lett.* 18(2), 1483 (2018)
20. X. Roy, C. H. Lee, A. C. Crowther, C. L. Schenck, T. Besara, R. A. Lalancette, T. Siegrist, P. W. Stephens, L. E. Brus, P. Kim, M. L. Steigerwald, and C. Nuckolls, Nanoscale atoms in solid-state chemistry, *Science* 341(6142), 157 (2013)
21. Y. Guo, Q. Du, P. Wang, S. Zhou, and J. Zhao, Two-dimensional oxides assembled by M_4 clusters (M= B, Al, Ga, In, Cr, Mo, and Te), *Phys. Rev. Res.* 3(4), 043231 (2021)
22. Q. Du, Z. Wang, S. Zhou, J. Zhao, and V. Kumar, Searching for cluster Lego blocks for three-dimensional and two-dimensional assemblies, *Phys. Rev. Mater.* 5(6), 066001 (2021)
23. X. Chen, G. Fei, Y. Song, T. Ying, D. Huang, B. Pan, D. Yang, X. Yang, K. Chen, X. Zhan, J. Wang, Q. Zhang, Y. Li, L. Gu, H. Gou, X. Chen, S. Li, J. Cheng, X. Liu, H. Hosono, J. Guo, and X. Chen, Superatomic-charge-density-wave in cluster-assembled $Au_6Te_{12}Se_8$ superconductors, *J. Am. Chem. Soc.* 144(45), 20915 (2022)
24. S. Xing, L. Wu, Z. Wang, X. Chen, H. Liu, S. Han, L. Lei, L. Zhou, Q. Zheng, L. Huang, X. Lin, S. Chen, L. Xie, X. Chen, H. J. Gao, Z. Cheng, J. Guo, S. Wang, and W. Ji, Interweaving polar charge orders in a layered metallic superatomic crystal, *Phys. Rev. X* 12(4), 041034 (2022)
25. Y. Zhao, Y. Guo, Y. Qi, X. Jiang, Y. Su, and J. Zhao, Coexistence of ferroelectricity and ferromagnetism in fullerene-based one-dimensional chains, *Adv. Sci. (Weinh.)* 10(21), 2301265 (2023)
26. J. R. Dilworth, Rhenium chemistry – then and now, *Coord. Chem. Rev.* 436, 213822 (2021)
27. K. Dehnicke and J. Straehle, N-Halogenoimido complexes of transition metals, *Chem. Rev.* 93(3), 981 (1993)
28. W. Liese, K. Dehnicke, I. Walker, and J. Strähle, Darstellung, eigenschaften und kristallstruktur von rhenium (VII)-nitridchlorid, $ReNCl_4$, *Z. Naturforsch. B. J. Chem. Sci.* 34(5), 693 (1979)
29. G. Kresse and J. Furthmüller, Efficient iterative schemes for ab initio total-energy calculations using a plane-wave basis set, *Phys. Rev. B* 54(16), 11169 (1996)
30. G. Kresse and D. Joubert, From ultrasoft pseudopotentials to the projector augmented-wave method, *Phys. Rev. B* 59(3), 1758 (1999)
31. J. P. Perdew, K. Burke, and M. Ernzerhof, Generalized gradient approximation made simple, *Phys. Rev. Lett.* 77(18), 3865 (1996)
32. J. Heyd, G. E. Scuseria, and M. Ernzerhof, Hybrid func-

tionals based on a screened Coulomb potential, *J. Chem. Phys.* 118(18), 8207 (2003)
33. S. Baroni, S. de Gironcoli, A. Dal Corso, and P. Giannozzi, Phonons and related crystal properties from density-functional perturbation theory, *Rev. Mod. Phys.* 73(2), 515 (2001)
34. R. Krishnan, J. S. Binkley, R. Seeger, and J. A. Pople, Self-consistent molecular orbital methods. XX. A basis set for correlated wave functions, *J. Chem. Phys.* 72(1), 650 (1980)
35. M. Dolg, U. Wedig, H. Stoll, and H. Preuss, Energy-adjusted ab initio pseudopotentials for the first row transition elements, *J. Chem. Phys.* 86(2), 866 (1987)
36. M. Frisch, G. Trucks, H. Schlegel, G. Scuseria, M. Robb, J. Cheeseman, G. Scalmani, V. Barone, G. Petersson, and H. Nakatsuji, Gaussian 16, Revision A. 03, Gaussian, *Inc. Wallingford CT* 3 (2016)
37. T. Tsukamoto, N. Haruta, T. Kambe, A. Kuzume, and K. Yamamoto, Periodicity of molecular clusters based on symmetry-adapted orbital model, *Nat. Commun.* 10(1), 3727 (2019)
38. G. Henkelman, A. Arnaldsson, and H. Jónsson, A fast and robust algorithm for Bader decomposition of charge density, *Comput. Mater. Sci.* 36(3), 354 (2006)
39. M. Segall, R. Shah, C. J. Pickard, and M. Payne, Population analysis of plane-wave electronic structure calculations of bulk materials, *Phys. Rev. B* 54(23), 16317 (1996)
40. D. Xiao, M. C. Chang, and Q. Niu, Berry phase effects on electronic properties, *Rev. Mod. Phys.* 82(3), 1959 (2010)
41. E. Bruyer, D. Di Sante, P. Barone, A. Stroppa, M. H. Whangbo, and S. Picozzi, Possibility of combining ferroelectricity and Rashba-like spin splitting in monolayers of the 1T-type transition-metal dichalcogenides MX_2 (M= Mo, W; X= S, Se, Te), *Phys. Rev. B* 94(19), 195402 (2016)
42. R. Fei, W. Kang, and L. Yang, Ferroelectricity and phase transitions in monolayer group-IV monochalcogenides, *Phys. Rev. Lett.* 117(9), 097601 (2016)
43. W. Wan, C. Liu, W. Xiao, and Y. Yao, Promising ferroelectricity in 2D group IV tellurides: A first-principles study, *Appl. Phys. Lett.* 111(13), 132904 (2017)
44. R. E. Cohen, Origin of ferroelectricity in perovskite oxides, *Nature* 358(6382), 136 (1992)
45. K. J. Choi, M. Biegalski, Y. L. Li, A. Sharan, J. Schubert, R. Uecker, P. Reiche, Y. B. Chen, X. Q. Pan, V. Gopalan, L. Q. Chen, D. G. Schlom, and C. B. Eom, Enhancement of ferroelectricity in strained $BaTiO_3$ thin films, *Science* 306(5698), 1005 (2004)
46. J. Rouquette, J. Haines, V. Bornand, M. Pintard, P. Papet, W. G. Marshall, and S. Hull, Pressure-induced rotation of spontaneous polarization in monoclinic and triclinic $PbZr_{0.52}Ti_{0.48}O_3$, *Phys. Rev. B* 71(2), 024112 (2005)
47. N. Izyumskaya, Y. I. Alivov, S. J. Cho, H. Morkoç, H. Lee, and Y. S. Kang, Processing, structure, properties, and applications of PZT thin films, *Crit. Rev. Solid State Mater. Sci.* 32(3–4), 111 (2007)
48. I. Bersuker, The Jahn–Teller Effect and Vibronic Interactions in Modern Chemistry, Springer Science & Business Media: 2013
49. J. van den Brink and D. I. Khomskii, Multiferroicity due to charge ordering, *J. Phys.: Condens. Matter* 20(43), 434217 (2008)
50. Y. Bao and F. Zhang, Electronic engineering of ABO_3 perovskite metal oxides based on d^0 electronic-configuration metallic ions toward photocatalytic water splitting under visible light, *Small Struct.* 3(6), 2100226 (2022)
51. J. C. Wojdeł and J. Íñiguez, Testing simple predictors for the temperature of a structural phase transition, *Phys. Rev. B* 90(1), 014105 (2014)
52. G. Kresse and J. Hafner, Ab initio molecular dynamics for liquid metals, *Phys. Rev. B* 47(1), 558 (1993)
53. K. A. N. Duerloo, M. T. Ong, and E. J. Reed, Intrinsic piezoelectricity in two-dimensional materials, *J. Phys. Chem. Lett.* 3(19), 2871 (2012)
54. K. M. Ok, E. O. Chi, and P. S. Halasyamani, Bulk characterization methods for non-centrosymmetric materials: Second-harmonic generation, piezoelectricity, pyroelectricity, and ferroelectricity, *Chem. Soc. Rev.* 35(8), 710 (2006)